https://doi.org/10.5194/egusphere-2026-2568
Preprint. Discussion started: 12 August 2026

WaggleDop: Autonomous event characterization and adaptive scanning using Doppler LiDAR systems

Robert Jackson[1], Paytsar Muradyan[1], Raghavendra Krishnamurthy[2], Rob Newsom[2], Sonia Wharton[3], Matteo Puccioni[3], Bhupendra Raut[1], Seongha Park[1], Rajesh Sankaran[1], Scott Collis[1], Joseph O'Brien[1], and V. Rao Kotamarthi[1]

[1]Argonne National Laboratory, 9700 Cass Ave., Lemont, IL, 60439
[2]Pacific Northwest National Laboratory, 902 Battelle Blvd, Richland, WA 99354
[3]Lawrence Livermore National Laboratory, 7000 East Ave, Livermore, CA 94550

Correspondence: Robert Jackson (rjackson@anl.gov)

Abstract. Adaptive scanning plays a key role in balancing observational strategies to address diverse scientific objectives while maximizing data collection for weather phenomena of interest. Current adaptive scanning capabilities for pulsed Doppler LiDARs (model Streamline XR), aimed at probing the streamwise velocity of atmospheric boundary layer flows, are limited to predefined scans based on wind directions derived from short-term wind profiles measured by the same instrument. As a result, high data rejection rates characterize the post-campaign phase due to excessive wind direction misalignment. To expand the Streamline LiDAR's adaptive scanning capabilities, we designed a novel WaggleDop instrument. WaggleDop is an edge computing-enabled system for adaptive scan that supports external inputs and multi-LiDAR configurations via cloud-native infrastructure. In this paper, we test the WaggleDop-LiDAR setup by studying 20 low level jet events and 19 wind reversal events resolved during two U.S. Department of Energy (DOE)-funded field campaigns. We demonstrate that WaggleDop successfully captured these events through adaptive scanning strategies that could not be implemented via classic standalone LiDAR setup, resulting in a substantial enhancement in data availability of up to 90%. The results shown here demonstrate the importance of more sophisticated scan adaptations to probe complex atmospheric boundary layer flows.

1 Introduction

The experimental characterization of the diurnal atmospheric boundary layer (ABL) evolution is crucial to support accurate weather forecasting. Low level jets (LLJs) or distinct wind speed maxima inside the ABL are examples of 3D complex flows influencing turbulent mixing and ABL evolution through vertical wind shear that require careful observational planning and execution. Forecasting these phenomena remains challenging for numerical weather prediction (NWP) models, whether in complex onshore terrain or within the marine ABL. To address this challenge, the U.S. Department of Energy (DOE) has led

https://doi.org/10.5194/egusphere-2026-2568
Preprint. Discussion started: 12 August 2026

several observational field campaigns aimed at improving our collective understanding of atmospheric processes within the ABL (Bodini et al., 2025).

Over the past decade, the US DOE and the National Oceanic and Atmospheric Administration (NOAA) have sponsored three Wind Forecast Improvement Projects (WFIPs) aimed at improving the High Resolution Rapid Refresh (HRRR) model (Benjamin et al., 2016), including predictions of LLJs. WFIP1 was a 1-year campaign that focused on characterizing the turbulent processes and LLJs in the ABL in the Great Plains over relatively flat terrain (Wilczak et al., 2015). WFIP2 was an 18-month campaign that focused its efforts on improving wind forecasts in the complex terrain of the Pacific Northwest (Wilczak et al., 2019). WFIP3 was an 18-month project to collect observations for improving wind forecasts over the coastal areas of New England (Kirinchich et al., 2026). Additionally, the DOE has funded a series of field campaigns collectively known as LiDAR Experiments for Assessing Flow over Forests (LEAFF) to study wind and improve the forecasting of lower boundary layer winds over canopy-covered complex terrain (Puccioni et al., 2025).

For each of these DOE-funded projects, the Halo Photonics Streamline XR+ Doppler LiDARs (DL) provided high-resolution wind measurements by retrieving the radial velocity (v_r) of aerosol particles in the direction of the emitted laser beam (Pearson et al., 2009). For many of these campaigns, the scanning strategies for the DL were frequently geared towards obtaining wind profiles and turbulence statistics over a single column (Krishnamurthy et al., 2025). Such strategies included vertical stare scans to obtain profiles of vertical velocity (w) and profiles of horizontal wind speeds calculated from velocity azimuth display (VAD) and Doppler beam swinging (DBS) scans (Newsom and Krishnamurthy, 2022; Krishnamurthy et al., 2021). These strategies provided high-frequency (0.2 to 1 Hz) observations of vertical wind profiles above the observation site that are crucial for validating wind forecasts from NWP models. However, these strategies do not capture the horizontal variability of winds or terrain- or canopy-induced flows. For example, LLJ wind velocities can exhibit significant horizontal variability in intensity over the open ocean on the scales of hundreds of meters (Edson et al., 2007; Wang et al., 2018). Therefore, observations of LLJ wind velocities over the open ocean are crucial for improving surface wind forecasts. Additionally, wind flow over complex orography can induce spatially-variable mountain waves (Draxl et al., 2021), katabatic/anabatic winds, and mountain-valley flow reversals (Whiteman, 1990; Stull, 2012; Fritts and Alexander, 2003). Large, multi-institution field campaigns studying these terrain-induced features, such as the WFIP2 (Wilczak et al., 2019), Terrain-induced Rotor Experiment (Grubišić et al., 2008; Wekker and Mayor, 2009; Doyle et al., 2009; Hill et al., 2010; Wang et al., 2025) and more recently the multi-scale Transport and Exchange processes in the Atmosphere over Mountains eXperiment (TEAMx) (Rotach et al., 2022) have used combinations of DLs to capture the high frequency wind statistics for turbulence as well as three-dimensional volumetric scans from DLs to capture the spatiotemporal features of flow in mountainous terrain. These examples show that there are often multiple science goals within a field campaign that have different sampling methodologies needed for a LiDAR network.

WFIP3 and LEAFF are examples of field campaigns with science goals that require different scan strategies for the same set of LiDARS. With a limited number of sensors available for a given project, choosing scan strategies that balance competing science goals of a field campaign is challenging. Typically, addressing multiple science questions (namely A and B) involves regular forecast briefings to determine the scan strategies based on expected weather conditions for the forecast period. In addition, having a fixed scan strategy to address Science Question A for the forecast period carries the risk of missed opportu-

https://doi.org/10.5194/egusphere-2026-2568
Preprint. Discussion started: 12 August 2026

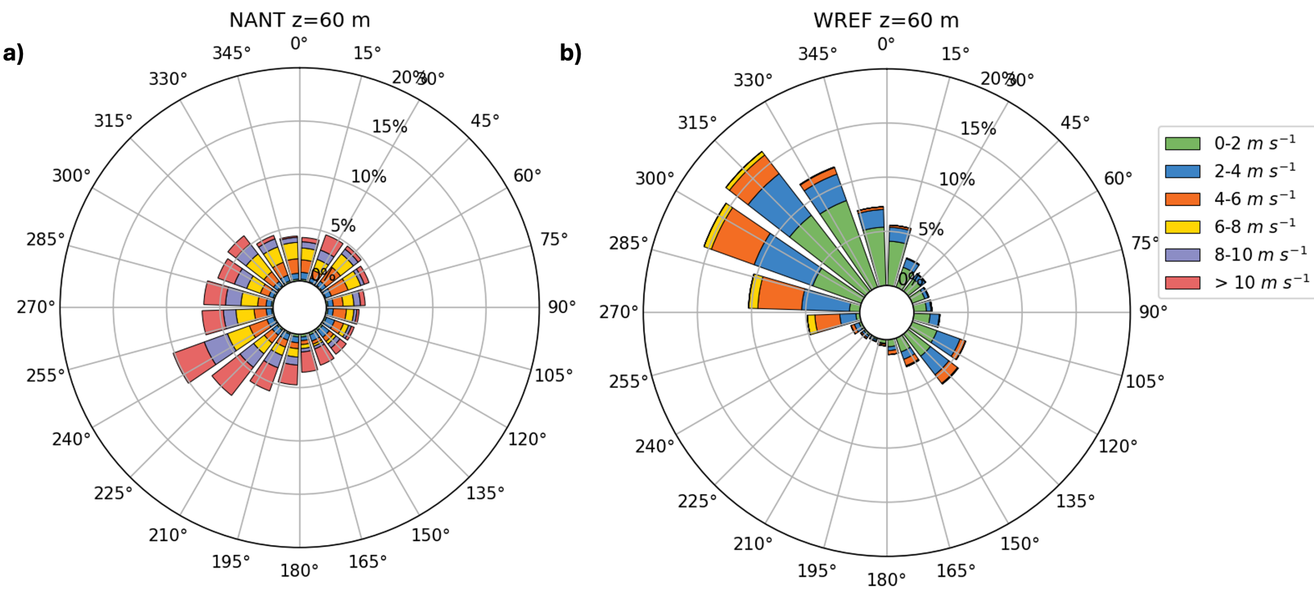

Figure 1. Wind roses at 60 m altitude above ground level from **(a)** the Nantucket Sewage Treatment Facility (NANT) WFIP3 and **(b)** WREF LEAFF site. All observations taken during their respective deployments are considered.

nities to adapt the scan strategy to answer Science Question B. Therefore, there is a need to adaptively select a scan strategy based on environmental conditions, a concept known as *adaptive scanning*. Adaptive scanning systems such as the Collaborative Adaptive Sensing of the Atmosphere (CASA; Brotzge et al., 2006) and the Multiangle Agile Adaptive Sensing system (MAAS; Kollias et al., 2020; Lamer et al., 2022, 2023) have been successfully implemented for scanning weather radars. To date, only Lamer et al. (2022) have demonstrated adaptive scanning of the DL with the MAAS framework, guiding the steering of a DL by a human operator using real-time input from a fisheye camera. In addition, the Scan Scheduler software on the DL's "DBS Feedback" mode allows for automatic adjustment of the scan strategy based on the short-term wind direction at a user-specified level detected by the VAD scan. However, there is no automated support for using wind speed and direction measured by other instruments, and the specified scans must be for fixed wind direction intervals, limiting self-configuring capabilities. Meanwhile, there is wide variability in near-surface wind directions experienced at the WFIP3 measurement site (Fig. 1a). In particular, mountain-valley flow reversal events are commonplace in the Wind River Experimental Forest (WREF) (Fig. 1b) Therefore, enhancing the existing self-configuring adaptive scans for DLs is crucial for the comprehensive quantification of complex ABL events via long-term research field campaigns.

In this study, we developed and tested WaggleDop, an adaptive scanning system for the DL leveraging the Waggle edge computing system, described in Beckman et al. (2016), for the WFIP3 and LEAFF campaigns. We demonstrate that WaggleDop significantly improves data availability for LLJ and mountain-valley flow reversal detection compared to a classical DL setup. The remainder of this manuscript is organized as follows. Section 2 provides a brief summary of the WFIP3 and LEAFF

https://doi.org/10.5194/egusphere-2026-2568
Preprint. Discussion started: 12 August 2026

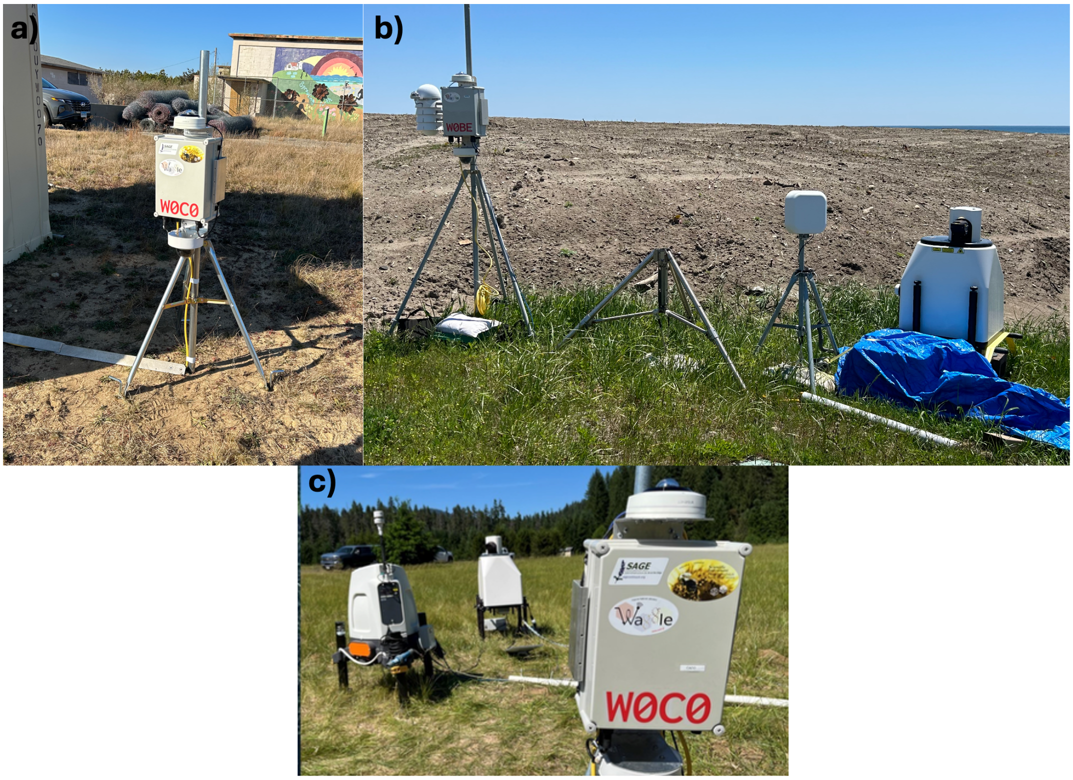

Figure 2. The Waggle Node installed at the (a) Cape Cod National Seashore (CACO) WFIP3 site, **(b)** Nantucket Sewage Treatment Facility (NANT) WFIP3 site, and **(c)** WREF LEAFF site. A sky-facing fish-eye camera is on the top of the node, while a ground-facing camera is at the bottom. The node's gray compute box hosts an NVIDIA NX compute module, power supply, and networking components.

campaigns and the relevant datasets for this study. Section 3 provides the details of the WaggleDop design. Section 4.1 shows initial test cases of the WaggleDop system over the WFIP3 Nantucket (NANT) and WREF LEAFF sites. Section 5 describes a test case characterizing mountain-valley flow reversals using WaggleDop during LEAFF. Section 6 discusses the advantages and challenges of the WaggleDop system for users to consider. Finally, the conclusions of the study are summarized in Section 7.

2 Experimental sites

During WFIP3, DLs were installed at various oceanic and coastal land sites on the Northeast Shelf of the U.S. East Coast (Kirinchich et al., 2026) (Figs. 2ab). For this study, we will focus on four DLs that were connected to Waggle Nodes, with their locations and standard operational scan strategies summarized in the first four rows of Table 1. These scan strategies are designed to capture the turbulent characteristics of the atmospheric boundary layer over a column (Banakh et al., 1999; Smalikho et al., 2005; O'Connor et al., 2010; Smalikho and Banakh, 2013, 2017; Bodini et al., 2018). Two primary scan

https://doi.org/10.5194/egusphere-2026-2568
Preprint. Discussion started: 12 August 2026

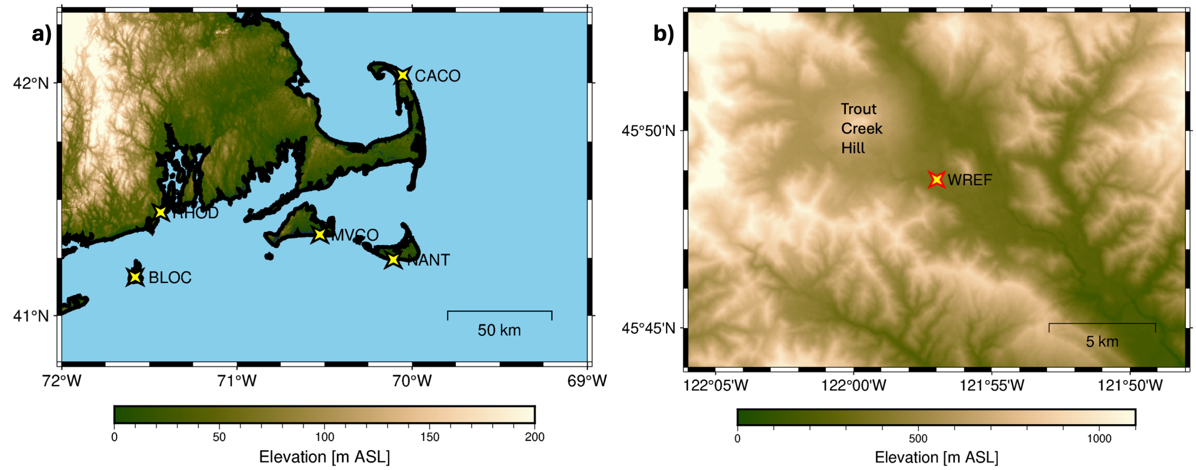

Figure 3. The map of the WFIP3 **(a)** and **(b)** LEAFF deployment sites. WFIP3 sites are located at coastal regions throughout the U.S. North East. WREF is located in southern Washington State towards the north end of a 23 km long valley which emerges into the Columbia River Gorge about 15 km south of the site.

strategies are listed in Table 1. The first is a continuous vertical stare, in which the DL points at zenith and records the signal-to-noise ratio (SNR) and radial velocity (v_r) with 30 m vertical resolution and 2 Hz frequency. In this paper, $v_r > 0$ represents motion away from the LiDAR. The second strategy is a VAD consisting of six vertical beams at 60° elevation, split evenly along the azimuth.

Table 1. Serial numbers, site IDs, and scan strategies of the Streamline XR lidars considered in this study.

Lidar ID	**Site ID**	**Scan strategy**
210	CACO	Hourly cycle: 50 min continuous VAD scans, followed by 10 min vertical stares
184	NANT	Continuous VAD scans (∼0.1 Hz)
216	BLOC	Continuous vertical stares (2 Hz)
217	BLOC	Continuous VAD scans (∼0.1 Hz)
190	LEAFF	Sector scans at 5°, 10°, and 15°, with 30° RHI scans

The above-mentioned DLs were installed at two sites for the WFIP3 campaign. The CACO site is located at the Highlands Center at the Cape Cod National Seashore about 90 m from the coast and about 10 km southeast of Provincetown, MA (Fig. 3a). The NANT site is located at the Nantucket Surfside Wastewater Treatment facility (Fig. 3a), about 90 m from the southern coast of Nantucket. Both of these sites, therefore, had the capability of sampling the effects of the sea-to-land transition on the spatial evolution of the LLJ. The BLOC site is located about 1 km north of the southern coast of Block Island at Block Island

https://doi.org/10.5194/egusphere-2026-2568
Preprint. Discussion started: 12 August 2026

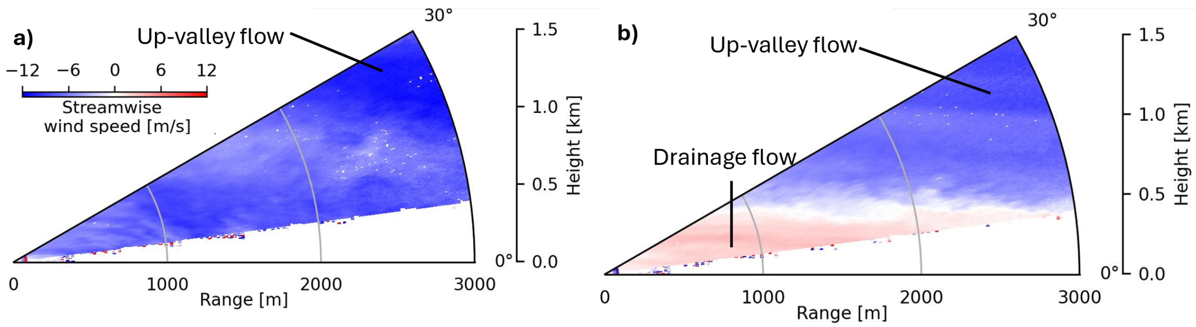

Figure 4. Vertical ABL flow evolution probed by the DL at WREF LEAFF on August 19, 2023. **(a)**: Diurnal flow (local time 12:00). **(b)** Nocturnal flow (local time 08:00). For both scans, the azimuth angle is 120° from North.

State Airport (Fig. 3a). At this location, we expect an increased influence of land surface roughness on onshore flows compared to the other sites, but there is still a capability to observe nocturnal LLJs that commonly occur at coastal sites. For all of the Waggle Nodes at these sites, we used an AT&T 5G SIM card for internet connectivity.

For LEAFF, two distinct regions were chosen for studying the impacts of forest canopies: one in the Appalachian Mountains of Virginia and another in the mountain-valley terrain of the Cascade Range in Washington. In this study, WaggleDop was deployed at the WREF site in the Cascade Range Region near Stabler, WA (Figs. 2c and 3b) and co-located with a National Ecological Observatory Network (NEON) 74 m tall flux tower. This site is located in a NW-SE running valley surrounded by forested mountains making it a favorable location for observing katabatic/anabatic flows and along axis valley flow reversals.

At WREF, a ZX300 profiling LiDAR and a DL were installed in a clearing to observe turbulence and the 2-D structure of these spatially-variable flows (Fig. 2b). In addition, a Waggle Node was connected to the DL, with internet connectivity enabled by Starlink. A previous experimental campaign involving one DL was conducted in Summer 2023 to spatially resolve the day- and night-time flow features over vertical transects probed by RHI. Examples of daytime valley flows and nighttime/early morning katabatic flows probed during the 2023 campaign are reported in Fig. 4a and 4b, respectively. The daytime valley flow (Fig. 4a) exhibits classic ABL flow features, i.e. monotonically increasing wind speed (up to $\approx 15\,\mathrm{m\,s^{-1}}$) and limited wind direction veer ($< 20°$, not shown here). By contrast, the early-morning ABL features lower velocity ($< 10\,\mathrm{m\,s^{-1}}$) and a complete flow reversal from drainage flows (katabatic flow/down-valley flow) in the bottom ABL to up-valley flow in the upper ABL. These three-dimensional complex flow features, and the associated rapid wind direction changes, justify the necessity of a real-time adapting scan strategy at WREF.

3 WaggleDop design

This section describes WaggleDop's design and workflow. In order to perform adaptive scanning, at least one DL and one Waggle Node are required. The DL connects to one of the Waggle Node's Power over Ethernet (PoE) ports via an external Wide Area Network (WAN) access port. With two PoE cameras already connected (Figs. 2abc), the Waggle Node has two

https://doi.org/10.5194/egusphere-2026-2568
Preprint. Discussion started: 12 August 2026

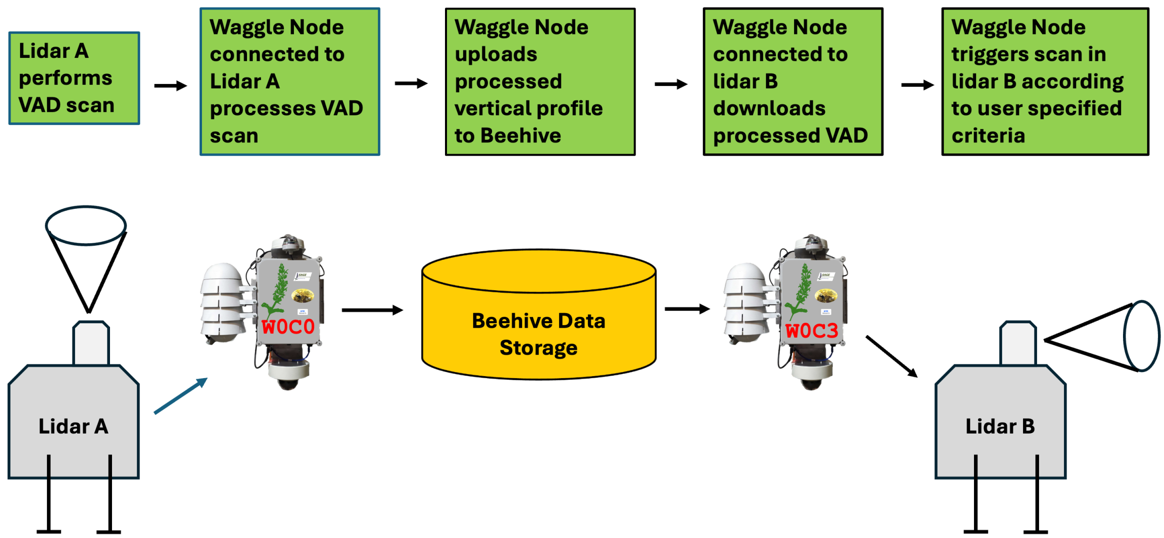

Figure 5. Flowchart demonstrating the workflow of the WaggleDop system.

available PoE ports, allowing up to two DLs to be connected to the same node. For external communications, the Waggle Node must either be connected to the Internet through Ethernet connected to its WAN port, a local WiFi network, or by using the internal modem that utilizes a SIM card to communicate over a 4/5G cellular connection. Finally, OpenSSH must be enabled on the DL in order for the Waggle Node to communicate with the DL via a Secure File Transfer Protocol (SFTP).

WaggleDop uses two Waggle plugins for its operation. The first, *windprofile*, computes the zonal (u) and meridional (v) components of the wind vector from the v_r collected by the latest VAD scan with the method outlined in Newsom et al. (2017). Before calculating the vertical profiles of u and v, each gate with an instantaneous SNR of less than -21.0 dB is filtered out, following Newsom et al. (2017), to ensure that the DL gates used to calculate the vertical profile contain returns from scatterers rather than noise. Once the vertical profile is calculated, the location and magnitude of the wind profile maximum below 1 km are determined as the LLJ nose location and magnitude. In addition, the wind speed and direction at a user-specified level are also uploaded. The resulting vertical profile and LLJ statistics are then uploaded to the Beehive (cloud server) (Fig. 5). In order to have these vertical profiles available in real time, the *windprofile* needs to be scheduled to run every minute using the Edge Scheduler at https://portal.sagecontinuum.org/jobs/my-jobs.

The second plugin, *lidarcontrol*, will download the latest vertical profile uploaded by a specified Waggle Node from the Beehive (Fig. 5). It then chooses between two possible Continuous Scanning Mode (CSM) files, using user-specified criteria regarding the wind direction range and minimum wind speed of the LLJ nose, as well as the wind speed and direction at a user specified height. The first file is a user-specified scan that will be sent to the DL if the user-specified criteria are met. The

https://doi.org/10.5194/egusphere-2026-2568
Preprint. Discussion started: 12 August 2026

second file is the control scan, typically a vertical stare or a VAD. WaggleDop currently supports creating user-specified Range Height Indicator (RHI) and stacked Plan Position Indicator (PPI) scans through a simple command line interface. Through these plugins, WaggleDop supports adaptive scanning over both single- and multi-LiDAR configurations. The user must schedule this plugin on the Edge Scheduler at fixed time intervals to continuously update the triggered scan.

3.1 Streamline XR doppler LiDAR operating modes

The DL operates in two modes. One mode of operation is through a pre-set schedule of scans as set in the Scan Scheduler software. The LiDAR will follow a loop of up to 8 possible scans: stare, VAD, RHI, 6-point VAD, and 4 User-specified scans (User1, User2, User3, User4). All scans except the Stare scan can be enabled or disabled by the user. Each scan can be scheduled to repeat at a user-specified interval. In addition, if an operator wants to operate all scans in order continuously, they set them to operate every 65535 seconds. An operator can also choose a single scan to operate continuously, bypassing the Stare scan in this mode. For each interval, the Scan Scheduler will automatically adjust the scan interval if the prescribed set of scan intervals causes any scan not to finish within the specified amount of time. When the scan is finished, the LiDAR will return to Stare mode until the next scheduled scan starts. If there are no user-scheduled scans, the LiDAR will continuously perform zenith pointing scans.

All of the User-type scans can be provided in two different formats, depending on how the user wishes to perform the scans. The first mode, step/stare, makes the LiDAR perform steps between specified azimuth and elevation angle pairs. When the LiDAR reaches the specified azimuth and elevation in the file, it will perform a long enough stare to collect a user specified number of rays before performing the next step. In this mode, only the rays at the specified azimuths and elevations are included, with transition gates removed. The other mode, CSM, is operated through a file that controls the speed, acceleration, and final azimuths and elevations of specified waypoints. The advantage of this mode compared to step/stare mode is finer control of the rotation speed of the LiDAR beam than in step/stare mode. Therefore, this mode is most appropriate for RHIs and PPI scans where continuous transitions at user-specified rotational speeds are required. A constant number of rays is saved in each ray, with potential antenna transition gates being saved since the LiDAR is in continuous operation mode. Starting with v16 of the Scan Scheduler software, User4 can be set to "Dynamic CSM" mode. In this mode, the User4 scan can be changed immediately upon changing two text files if the User4 scan is set to operate continuously. This provides the advantage of immediate scan triggering but can also interrupt the current scan.

3.2 Single-LiDAR configuration

Adaptive scanning on a single LiDAR follows the flowchart given in Fig. 5, where LiDARs A and B are the same LiDAR. For configuring adaptive scanning on a single LiDAR, there are two modes of operation supported by *lidarcontrol*, with the tradeoffs of each listed in Table 2. First, *lidarcontrol* can change the scheduled scan as User1. Unless the LiDAR is set to continuously perform the scan in User1, this requires a minimum of two minutes between the start of two triggered scans. However, operating the User1 scan continuously eliminates the possibility of combining vertical stare scans and adaptive scanning on a single Streamline XR DL. Therefore, the user must consider this tradeoff when performing adaptive scanning

https://doi.org/10.5194/egusphere-2026-2568
Preprint. Discussion started: 12 August 2026

using a single LiDAR with WaggleDop under scheduled scan mode. Under the scheduled scan mode, the scan will not start until all previously scheduled scans are complete. This eliminates the possibility of interrupting a triggered scan at the cost of finer control of the triggered scan time.

Secondly, *lidarcontrol* supports Dynamic CSM mode, a feature that requires v16 or later of the Scan Scheduler software to be installed on the LiDAR. It allows for immediate triggering of a scan in User4 if the LiDAR is set to continuously perform the User4 scan. This provides the advantage of immediate triggering. However, scans can be interrupted mid-stream through remote triggering, so one must consider this when determining the time interval that the *lidarcontrol* plugin is scheduled to run. Running *lidarcontrol* during Dynamic CSM mode at a shorter scheduled interval enables more frequent scan updates at the cost of interrupting scans. Running *lidarcontrol* at less frequent intervals mitigates the scan interruption issue at the cost of reducing the frequency of scan updates.

3.3 Multi-LiDAR configuration

The multi-LiDAR configuration for a pair of LiDARs follows the same flowchart given in Fig. 5. Multiple, non-mutually exclusive LiDAR pairs can operate concurrently within a single campaign; therefore, the framework scales to an arbitrary number of LiDARs. The multi-LiDAR configuration can also run in Dynamic CSM and scheduled scan mode, with the tradeoffs between the two listed in Table 2. The multi-LiDAR configurations allow for continuous sampling of vertical profiles while performing adaptive scanning. If more than one DL is present in the network, then one LiDAR should perform VAD scans and the others should either have the User1 scan enabled or use Dynamic CSM mode with the User4 scan enabled. The same tradeoffs between the Dynamic CSM and scheduled scan mode for single-LiDAR configurations apply to multi-LiDAR configurations. Since this system operates with any DL connected to a Waggle Node, the two-LiDAR configuration also allows

	Dynamic CSM mode	**Scheduled scan mode**
Single-lidar advantages	Immediate control of triggered scans	Recommended mode for single-lidar adaptive scanning
Single-lidar disadvantages	No vertical stares; scans may be interrupted; not recommended for single-lidar operation	–
Multi-lidar advantages	Immediate control of individual lidar; no interruption of VAD scans on other systems	No interruption of triggered scans; with a dedicated VAD lidar, enables more frequent triggered scans
Multi-lidar disadvantages	Triggered scans may be interrupted	Must wait for completion of scheduled scans

Table 2. Trade-offs between Dynamic CSM and Scheduled Scan modes for different lidar configurations.

https://doi.org/10.5194/egusphere-2026-2568
Preprint. Discussion started: 12 August 2026

windprofile running on a Waggle Node connected at a separate field site to provide the wind profiles for *lidarcontrol* to trigger scans.

4 Results

4.1 Test case 1: Low-level jets over Nantucket

In this study, WaggleDop performed adaptive sampling experiments geared toward two different weather phenomena. First, WaggleDop automatically detected LLJs and performed adaptive scanning for a 7-day test over the Block Island (BLOC) and NANT sites during WFIP3. Nocturnal LLJs are a common atmospheric phenomenon that continue to pose challenges for accurate prediction (Shaw et al., 2022; Jiang and Edson, 2020). Therefore, this motivated testing WaggleDop on LiDARs configured in regions that experience nocturnal LLJs regularly.

For this experiment, we chose the multi-LiDAR configuration with scheduled scan mode in Table 2. For this we configured LiDAR SN 217 at BLOC to perform continuous VAD scans. The *windprofile* plugin, executed by the Waggle Node at BLOC, then continuously processed the v_r data from these VAD scans and uploaded the resultant wind profiles to the Beehive. In order to define the presence of a significant LLJ near the surface for adaptive scanning, two criteria were established:

- The 150 m wind speed at BLOC is > 10 m/s.
- The 150 m wind direction at BLOC is between 90° and 270° to ensure that we are capturing onshore flows.

The 150 m height is chosen to capture time periods when the LLJ is close to the surface and is most likely to impact surface weather conditions. If both criteria are met, LiDARs SN 184 (NANT) and 216 (BLOC) performed hemispherical range height indicator (HSRHI) scans along the 150 m wind direction to provide full 180° cross sections of v_r along the 150 m wind direction. If these criteria were not met, then these LiDARs performed vertical stares. LiDARs SN 216 and 184 were set to scheduled scan mode to ensure complete scans, with the *lidarcontrol* plugin running every 5 minutes. 89.8% of the time periods were not selected for triggering RHIs using this criterion, showing that adaptive scanning can significantly improve data availability over a set operational scan strategy.

Figure 6 shows a time series of the 150 m wind speed and direction as recorded by the DL SN 217 performing VAD profile scans. During this time period, 5 events were detected by WaggleDop from 05:00 LDT on 28 July 2025 until 05:00 LDT on 29 July 2025. For this test case, we will focus on the 3 events starting at 17:00 LDT on 29 July 2025 and ending at 21:00 LDT. The Waggle system was offline at 19:00 LDT for one hour, interrupting triggering. Otherwise, Fig. 6 shows that these LiDAR were triggered in unison to scan the same azimuth angle along the BLOC VAD LLJ nose direction, demonstrating that *lidarcontrol* successfully triggered the NANT LiDAR simultaneously, despite the BLOC and NANT sites being 100 km apart. In total, WaggleDop triggered 734 RHI scans during this time period, containing a dataset with 4° resolution v_r every 40 seconds.

The evolution of the streamwise velocity U in the LLJ captured by the NANT LiDAR HSRHI scans is shown in Fig. 7. For this figure, the v_r were converted to streamwise velocity U by first calculating $U = v_r/\cos\theta$, where θ is the elevation angle.

https://doi.org/10.5194/egusphere-2026-2568
Preprint. Discussion started: 12 August 2026

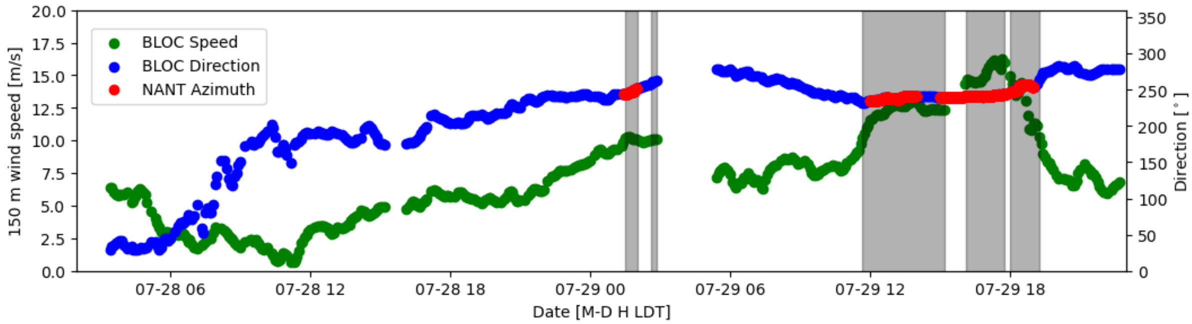

Figure 6. The 150 m wind speed (line) and direction from the BLOC VAD wind scans. The shaded gray regions indicated when WaggleDop triggered the NANT LiDAR to perform streamwise HSRHIs.

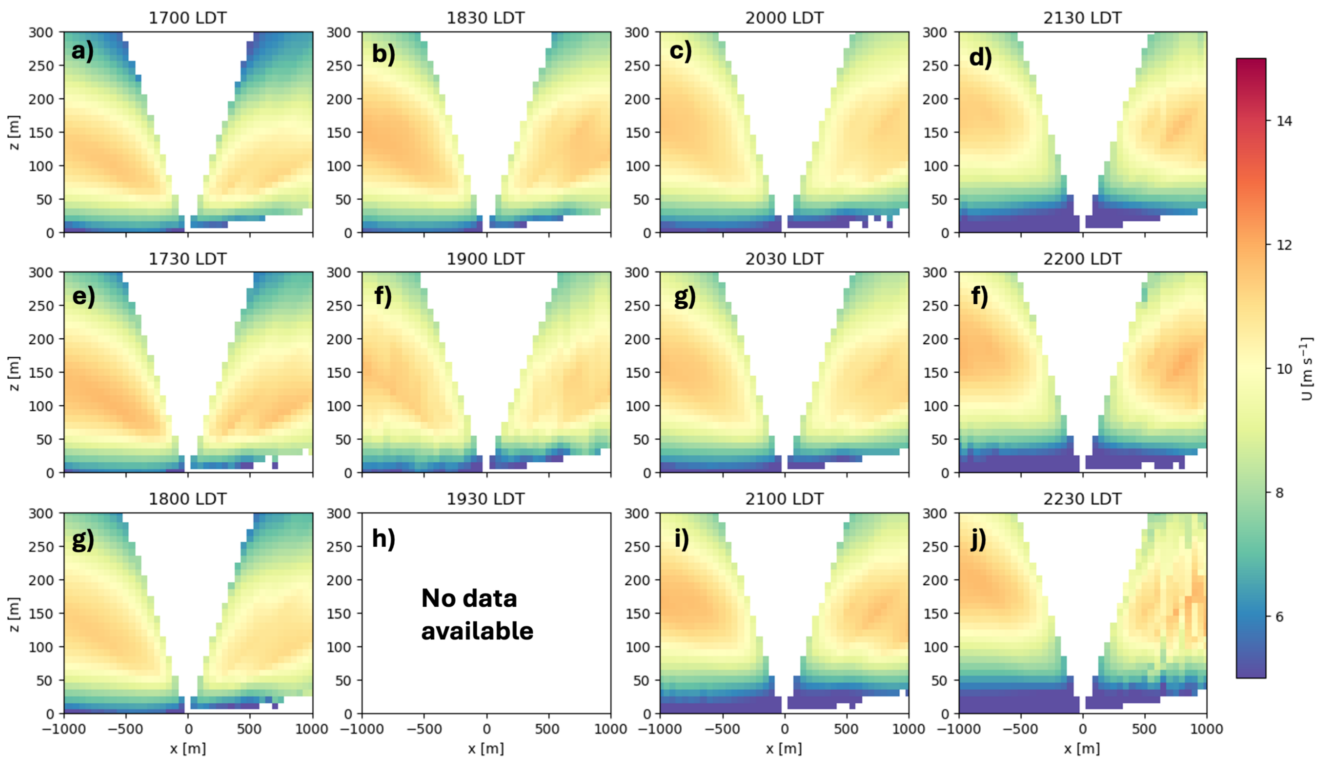

Figure 7. 30-minute averaged U from the WaggleDop-triggered RHI scans from 17:00 LDT to 22:30 LDT on July 29 2025. Positive x values point southward offshore. Subpanels **(a-j)** represent different 30-minute time intervals.

215 Then, all data where $20^\circ < \theta < 160^\circ$ were excluded to ensure that the vertical component of v_r is small, reducing uncertainty in U due to the vertical component of v_r. Next, all gates with instantaneous $SNR < -21.0$ dB were removed to eliminate noisy velocities. Then, the U for each timestep were interpolated to a Cartesian grid over the along-HSRHI axis x and height above

https://doi.org/10.5194/egusphere-2026-2568
Preprint. Discussion started: 12 August 2026

ground level z with $\Delta x = 50$ m and $\Delta z = 10$ m so that each scan is on a consistent spatial grid. In this coordinate system, $x > 0$ m is southward and offshore. Finally, we calculated 30 minute averages of U from the instantaneous observations, as shown in Fig. 7.

Starting at 17:00 LDT, U is below 12 $m\ s^{-1}$, with the maxima present from 50 m to 150 m above ground level. It is also evident that the winds onshore ($x > 0$ m) are stronger than the winds offshore ($x < 0$ m), with the vertical extent of the $U > 10\ m\ s^{-1}$ values higher by 25 m onshore (Fig. 7a-c). As the evening progresses, the discrepancy between the wind speeds onshore and offshore starts to narrow, with the $U > 10\ m\ s^{-1}$ values extending above $z = 200\ m$ both onshore and offshore through 20:00 LDT (Fig. 7g-i). By 22:00 LDT, the LLJ starts to rise, with the maximum U values rising above 150 m (Fig. 7j-l). Therefore, WaggleDop successfully captured the temporal evolution of the structure and spatial heterogeneity of the nocturnal LLJ near the surface during this test experiment.

5 Test case 2: Topographic flow reversals during LEAFF

Winds in the warmer summer months at WREF are usually influenced by strong thermal gradients that develop in the surrounding mountain-valley terrain (Fig. 3). LEAFF was designed to capture the predominant daytime/nighttime along-axis valley flow reversals (SE-NW) observed at the site (Wharton et al., 2017). To align the LiDAR scan with the ambient flow direction, LEAFF employed adaptive scanning in order to trigger the Streamline XR DL to scan both up and down the valley. To do this, we developed a set of rules that focused on sampling the lowest 150 m of the atmosphere, employing the single-LiDAR configuration in scheduled scan mode. For the entire LEAFF campaign (10 June to 15 September 2025), we configured the Streamline XR DL in continuous scanning operation mode that switched between a vertical Stare, a VAD scan, and a User1 scan for use by *lidarcontrol*. The User1 scan was changed by *lidarcontrol* on the following schedule:

- Every 6 minutes, starting at the top of the hour, *lidarcontrol* triggered a stacked sector scan that was $45°$ wide at 3 elevations: $5°$, $10°$, and $15°$. The center of each scan was taken along the wind direction at 142 m as taken from a VAD scan. The azimuthal rotation speed was set to $2°\ s^{-1}$, ensuring 22.5 seconds per elevation scan.

- Every 6 minutes, starting at minute 3 of each hour, *lidarcontrol* triggered an RHI from $10°$ to $30°$ along the 142 m wind direction from the DL VAD scans. The elevation rotation speed was set to $2°\ s^{-1}$, ensuring 10 seconds per RHI scan.

- If the wind direction was between $0°$ and $180°$, then $180°$ was added to the azimuth angle to ensure that we were sampling the vicinity of the mountains to the west of the site, including Trout Creek Hill (Fig. 3b).

This schedule permitted the changing of the scan type every three minutes between volume scans for greater spatial coverage and RHIs for greater frequency in studying mountain-valley flow dynamics.

We next focus on a single event where the flow switched from coming up valley to flowing down valley on a fair weather day. This event occurs on 29 July 2025 from 13:00 to 18:00 LDT as the shaded, sloped surfaces cool. The VADs show the flow reversing at 16:25 LDT (Fig. 8a). During this time, *lidarcontrol* successfully triggered the DL to scan along the flow direction,

https://doi.org/10.5194/egusphere-2026-2568
Preprint. Discussion started: 12 August 2026

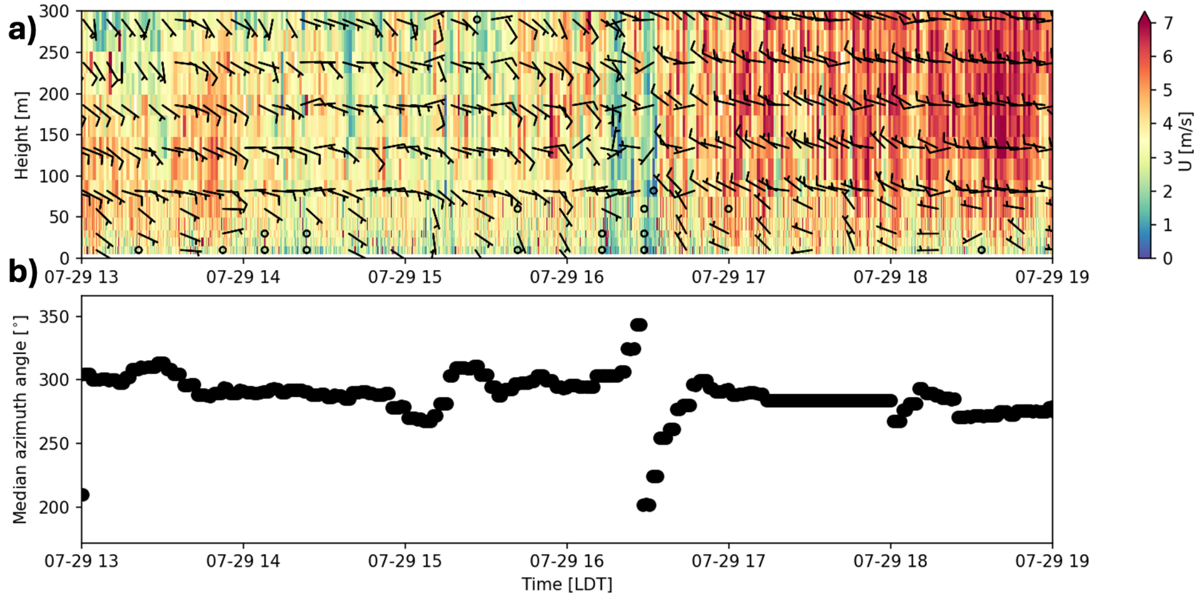

Figure 8. (a) The mean horizontal wind profiles overlaid over wind speed from the ZX-300 wind profiles (below 70 m AGL) and DL VAD scans (above 70 m AGL) during a flow reversal event on 29 July 2025 from 13:00 to 19:00 LDT. **(b)** The mean azimuth angle of the scans triggered by WaggleDop during this flow reversal event.

first upwind of the flow before 16:28 LDT and then downwind after that (Fig. 8). The range of median azimuth angles from the RHI and PPI scans is from 201° to 343° (Fig. 8b). Using a default scan strategy spanning 201 to 343 degrees for all three PPIs would take 71 seconds per elevation, or 3.55 minutes for all 3 elevations. Using WaggleDop's adaptive scanning capability brings the scan time down to 22.5 seconds per elevation scan, or 1.25 minutes per elevation scan. This shows how WaggleDop's adaptive scanning can increase data frequency in the up and down-valley flows by specifically adapting the scan to the flow direction. Furthermore, adapting both the RHI and PPI scans to the azimuth angle is impossible in DBS feedback mode, as only set scans can be defined in User4. Therefore, not only was adaptive scanning successful, but we demonstrate here that WaggleDop can provide a significant improvement in adaptive scanning capabilities compared to what is currently available in the Streamline LiDARs.

Figure 9 shows the temporal evolution of the valley flow as shown through hourly averaged v_r values from the 5° PPI scan in the vicinity of the DL. In order to generate Figure 9, we first removed each v_r value where the $SNR < -20.0\ dB$ to filter out noisy v_r values. Since each scan has a different set of radial coordinates, computing averages requires interpolating these scans to a Cartesian grid. Therefore, we linearly interpolated the v_r over a two-dimensional grid that spans 2.5 km in the along-flow (x) and vertical (z) directions, with $\Delta x = \Delta y = 10$ m. Overall, Figures 9a-c show positive v_r values through 16:00 LDT (Fig. 9a-c), representing southeasterly flow. At 16:00 LDT, the flow reversal event occurs, with both negative v_r values present in the hourly average at ranges up to 2 km (Fig. 9d). After 17:00 LDT, the negative v_r values are present within 2 km of the DL indicating that the flow near the DL has reversed (Fig. 9ef), showing northwesterly flow. Therefore, this shows that the flow

https://doi.org/10.5194/egusphere-2026-2568
Preprint. Discussion started: 12 August 2026

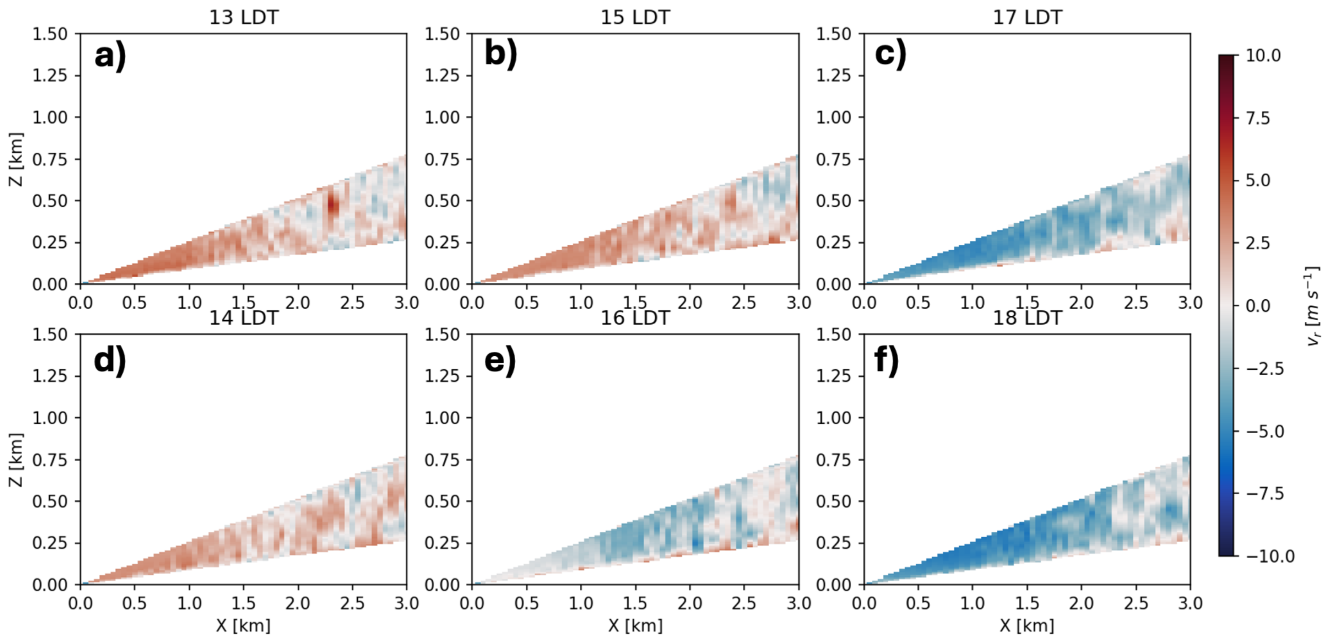

Figure 9. The hourly average v_r from the interpolated RHI scans. Sub panels **(a-f)** represent Hours 13:00 to 18:00 local daylight time (LDT).

reversal event, and the complex flows in the terrain surrounding the DL, were successfully captured by WaggleDop, with the scan strategy changing according to the wind direction.

6 Discussion and Challenges

The previous sections demonstrated some of WaggleDop's improved adaptive scanning capabilities compared to the DBS feedback mode already implemented in the Streamline LiDAR. For example, WaggleDop can trigger scans in the DL based on wind profiles from remote sites, presenting a dramatic improvement to the adaptive scanning capabilities currently supported by DBS Feedback mode that is presently supported by the Streamline LiDARs. Specifically, the DBS feedback mode only uses wind direction from a user specified height of a wind profile collected by the same LiDAR immediately before the scan, with no external inputs. Therefore, using a multiple-LiDAR configuration that triggers scans based on profiles from sites separated by over 100 km is impossible with the DBS Feedback mode, while WaggleDop enables such distributed, network-aware scanning seamlessly.

In addition, no wind speed criteria can be provided for DBS feedback mode. Even with the use of the 150 m wind criteria here, the lack of a wind speed criterion can cause the DBS feedback mode to trigger scans during low-wind conditions, when the wind direction vector would be uncertain and the data uninteresting for studying high wind events. This particular case was oriented towards scanning LLJs near the surface to study when it would be most impactful for forecasting surface high wind events. If one is interested in capturing the entire evolution of the LLJ, then using one fixed height for adaptive scanning is

https://doi.org/10.5194/egusphere-2026-2568
Preprint. Discussion started: 12 August 2026

inadequate, as shown in Figure 7. Therefore, WaggleDop's ability to process wind profiles from other LiDARs and determine the LLJ nose can be used to track the LLJ throughout its entire lifecycle.

With the DBS feedback mode, the user must also wait for the LiDAR to process the VAD scan raw data into wind profiles, which adds about 45 seconds of delay between obtaining the wind profile and performing the next scan. With WaggleDop, raw VAD data processing is done by the Waggle Node with a VAD scan entered as a user scan in step-stare mode. This allows the next scan to proceed sooner and, therefore, increases the scan frequency compared to the DBS feedback mode. Additionally, the user must pre-specify wind direction intervals with already-prescribed scans instead of generating scans on the fly. This makes it difficult to align azimuth angles for scans precisely, as potentially hundreds of CSM files must be pre-generated to take full advantage of the DBS feedback mode. WaggleDop allows the user to automatically generate these CSM files with ease, reducing the labor needed to perform adaptive scanning with the DLs. Finally, DBS Feedback mode does not allow the user to change the triggered scan type at set intervals. Therefore, the adaptive scanning experiment performed for LEAFF would have been impossible in DBS Feedback mode.

Designing and testing WaggleDop was not without challenges that the community should consider before deployment. For example, during the first experiment at NANT, we were able to trigger RHI scans along the LLJ nose direction, as detected by the BLOC LiDAR. However, due to a previously unknown azimuth offset, the NANT LiDAR scans were triggered to scan with a 80.8° offset from the 150 m wind direction. Therefore, the results shown here demonstrate the importance of coordinated calibration of all LiDARs being deployed as part of WaggleDop. Due to this challenge, WaggleDop supports implementing a user defined azimuth offset in its inputs to enable efficient coordination between LiDARs. This user defined azimuth offset was used to produce the WFIP3 data shown in Figures 6 and 7.

During the second experiment at WFIP3, the BLOC LiDAR successfully triggered RHI scans in the direction of the LLJ nose measured at BLOC. However, the BLOC LiDAR was not triggered, even though the job was started. This was likely due to issues with deploying the job on the Waggle infrastructure. Therefore, another challenge in performing adaptive scanning using WaggleDop may arise from occasional lapses in remote network connectivity and the availability of the Waggle cloud infrastructure (Beehive). Most often, the Waggle infrastructure was unavailable at 00:00 UTC for an hour. Therefore, We strongly recommend that, even though this process is mostly automated, regular monitoring of the data be performed to ensure full coordination and functionality of the WaggleDop system. Despite these challenges, both experiments captured the passage of 20 LLJs over BLOC and NANT.

For LEAFF, we were limited to using one DL. Using two or more LiDARs for adaptive scanning is highly recommended, as one LiDAR can provide vertical profiles or other inputs for WaggleDop, and the subsequent LiDARs can perform the scans without waiting for the VAD scans to finish. However, due to the proprietary nature of the data feed inside the ZX300, it was difficult to use its vertical profiles as inputs for WaggleDop. Instead, the profiling LiDAR data provides post-experimental reference observations of the wind direction. We also did not investigate obtaining real-time 3D sonic anemometer data from the nearby NEON flux tower, which may have offered another directional source. Therefore, we were limited to a single scanning LiDAR for LEAFF, lowering the frequency of PPI and RHI scans. Despite these challenges, we were able to successfully capture 19 wind reversal events, including those that occurred under low wind conditions.

https://doi.org/10.5194/egusphere-2026-2568
Preprint. Discussion started: 12 August 2026

These experiments show that adaptive scanning using inputs from separate LiDARs connected to Waggle Nodes was successful as long as either an instrument's data feed is on the network or uploaded to the cloud using a Waggle plugin. Further development plans for WaggleDop include integrating data from other meteorological sensors. To that end, a plugin that uploads the Vaisala Weather Transmitter data to the Beehive already exists and is used for the CROCUS Micronet and the Argonne Deployable Mast (Muradyan et al., 2026; Collis et al., 2025). This enables the quick expansion of WaggleDop to incorporate wind measurements from standard meteorological sensors connected to Waggle Node as inputs. Therefore, this system is expandable to utilize a large array of instruments as inputs for adaptive scanning. Future work on WaggleDop will, therefore, focus on using WXT and sonic anemometer measurements as inputs to WaggleDop.

7 Summary

Streamline XR Doppler LiDARs (DLs) are commonly used in wind and turbulence measurement campaigns to measure the turbulent characteristics of mountain-valley flows as well as low level jets. Typically, the scan strategies for DLs are determined by the user ahead of time. However, choosing a particular scan strategy requires a tradeoff between temporal frequency and spatial coverage. This can complicate the decision regarding scan strategies for field campaigns that have scientific goals requiring both data with high temporal frequency and data with full volume scans. To automate the scan selection process for given scientific goals, we developed the WaggleDop system, initially implemented on the Streamline XR DL but designed to be instrument-agnostic. The framework can be implemented on any scanning DL that allows external scan control and configurable command interfaces. WaggleDop uses Argonne National Laboratory's Waggle Node, an edge computing device built on a cloud-native infrastructure that can store and communicate data processed at the point of the instrument.

WaggleDop is installable for a Streamline XR DL by connecting a Waggle Node to a Streamline XR Doppler LiDAR using an Ethernet connection. More generally, the system architecture only requires network-level communication with the LiDAR. The software of the WaggleDop system consists of two applications: one that processes vertical profiles and uploads them to the cloud for each LiDAR, and another that triggers DL scans based on the uploaded vertical profiles from any LiDAR.

We tested the WaggleDop system during two Department of Energy-funded field campaigns: the 3rd Wind Forecast Improvement Project (WFIP3) and LiDAR Experiments for Assessing Flow over Forests (LEAFF). We show here that we can successfully use a multi-LiDAR setup, where one LiDAR is set to obtain vertical wind profiles and the other is set to perform adaptive scanning of low level jets based on the profiles of the DL, which is set to perform continuous Velocity Azimuth Display scans. In addition, we have successfully collected data throughout an entire summer campaign, sampling orographic flows while adapting to the reversal of flows associated with differential solar heating and radiative cooling induced by complex terrain. We have demonstrated sampling strategies through WaggleDop's capabilities that would have been impossible using the current capabilities of the Streamline LiDARs. This was accomplished by using data from external sources as criteria for triggering and its ability to change the prescribed scan for a given set of azimuth angles through remote triggering.

Future work on WaggleDop includes the integration of other wind sensors, such as radar wind profilers, profiling LiDARs, weather transmitters, and sonic anemometers. In addition, efforts are currently underway to couple the WaggleDop system with

https://doi.org/10.5194/egusphere-2026-2568
Preprint. Discussion started: 12 August 2026

artificial intelligence-based digital twins of Chicago (Kotamarthi et al., 2025) and lake breeze detection models for weather radars in Chicago (Park et al., 2026). Such efforts will create digital twins that can enhance real-time data collection and real-time weather forecasting. The work here shows the importance of adaptive scanning for improving data availability for sampling LLJs and mountain-valley flow reversals using DLs.

Code and data availability. The Streamline LiDAR data are available for download at the Wind Data Hub (https://wdh.energy.gov/) under DOIs 10.21947/3000130, 10.21947/2229436, 10.21947/2228815, and 10.21947/2583389. The Waggle plugins are available at on the Edge Computing Repository as *LiDARcontrol* (https://portal.sagecontinuum.org/apps/app/rjackson/LiDAR-control) and *windprofile* (https://portal.sagecontinuum.org/apps/app/rjackson/windprofile). Writefull, an AI-based grammar checking tool, was used to improve the grammar and readability of the manuscript.

Author contributions. Authors RJ, PM, SW and MP contributed to the data analysis. Authors RJ, PM, RN, SW, MP, RS, and JO contributed to planning of the field deployments and installation of the instruments. Authors RJ, PM, RK, SW, SC, and VRK contributed to the proposal development for WFIP3, LEAFF, and the Incubator studies. Authors BR, RS and SP advised on developing workflows for the Waggle Node.

Competing interests. The authors have no conflicts of interest to disclose.

Acknowledgements. This material is based upon work supported by the U.S. Department of Energy, Office of Science, under contract number DE-AC02-06CH11357. This study is supported by the U.S. Department of Energy's Integrated Energy Systems Office's Incubator Program and the Observationally-based Resource Assessment and Coupled Modeling Annual Operating Plan under prime contracts DE-AC02-06CH11357, DE-AC52-07NA27344, and DE-AC05-76RL01830. We gratefully acknowledge the computing resources provided on Improv (and/or Bebop and/or Swing), a high-performance computing cluster operated by the Laboratory Computing Resource Center at Argonne National Laboratory. For MP and SW, this work was performed under the auspices of the U.S. Department of Energy by Lawrence Livermore National Laboratory under Contract DE-AC52-07NA27344 with release number LLNL-JRNL-2017629.

https://doi.org/10.5194/egusphere-2026-2568
Preprint. Discussion started: 12 August 2026

References

Banakh, V. A., Smalikho, I., Köpp, F., and Werner, C.: Measurements of Turbulent Energy Dissipation Rate with a CW Doppler Lidar in the Atmospheric Boundary Layer, Journal of Atmospheric and Oceanic Technology, 16, 1044 – 1061, https://doi.org/10.1175/1520-0426(1999)016<1044:MOTEDR>2.0.CO;2, 1999.

Beckman, P. H., Sankaran, R., Catlett, C., Ferrier, N. J., Jacob, R. L., and Papka, M. E.: Waggle: An open sensor platform for edge computing, 2016 IEEE SENSORS, pp. 1–3, https://api.semanticscholar.org/CorpusID:2797332, 2016.

Benjamin, S. G., Weygandt, S. S., Brown, J. M., Hu, M., Alexander, C. R., Smirnova, T. G., Olson, J. B., James, E. P., Dowell, D. C., Grell, G. A., et al.: A North American hourly assimilation and model forecast cycle: The Rapid Refresh, Monthly Weather Review, 144, 1669–1694, 2016.

Bodini, N., Lundquist, J. K., and Newsom, R. K.: Estimation of turbulence dissipation rate and its variability from sonic anemometer and wind Doppler lidar during the XPIA field campaign, Atmospheric Measurement Techniques, 11, 4291–4308, https://doi.org/10.5194/amt-11-4291-2018, 2018.

Bodini, N., Moriarty, P., Letizia, S., Mann, J., Wharton, S., Deskos, G., Doubrawa, P., Fast, J., Hamilton, N., Herges, T., Kaul, C., Kelley, C., Krishnamurthy, R., Lavin, L., Lundquist, J. K., Maniaci, D., and Naughton, J.: A perspective on lessons learned and future needs for wind energy field campaigns, Journal of Renewable and Sustainable Energy, 17, 032 302, https://doi.org/10.1063/5.0252362, 2025.

Brotzge, J. A., Droegemeier, K., and McLaughlin, D. J.: Collaborative Adaptive Sensing of the Atmosphere: New Radar System for Improving Analysis and Forecasting of Surface Weather Conditions, Transportation Research Record, 1948, 144–151, https://doi.org/10.1177/0361198106194800116, 2006.

Collis, S. M., Muradyan, P., Jackson, R., Raut, B. A., O'Brien, J. R., Tuftedal, M. E., Grover, M. A., Kotamarthi, V. R., and et al.: The CROCUS Urban Canyons Campaign: Multiscale Observations of the Canopy Layer and Urban Boundary Layer in Chicago, Bull. Amer. Meteor. Soc., manuscript under review, 2025.

Doyle, J. D., Grubišić, V., Brown, W. O. J., Wekker, S. F. J. D., Dörnbrack, A., Jiang, Q., Mayor, S. D., and Weissmann, M.: Observations and Numerical Simulations of Subrotor Vortices during T-REX, Journal of the Atmospheric Sciences, 66, 1229 – 1249, https://doi.org/10.1175/2008JAS2933.1, 2009.

Draxl, C., Worsnop, R. P., Xia, G., Pichugina, Y., Chand, D., Lundquist, J. K., Sharp, J., Wedam, G., Wilczak, J. M., and Berg, L. K.: Mountain waves can impact wind power generation, Wind Energy Science, 6, 45–60, https://doi.org/10.5194/wes-6-45-2021, 2021.

Edson, J., Crawford, T., Crescenti, J., Farrar, T., Frew, N., Gerbi, G., Helmis, C., Hristov, T., Khelif, D., Jessup, A., Jonsson, H., Li, M., Mahrt, L., McGillis, W., Plueddemann, A., Shen, L., Skyllingstad, E., Stanton, T., Sullivan, P., Sun, J., Trowbridge, J., Vickers, D., Wang, S., Wang, Q., Weller, R., Wilkin, J., Williams, A. J., Yue, D. K. P., and Zappa, C.: The Coupled Boundary Layers and Air–Sea Transfer Experiment in Low Winds, Bulletin of the American Meteorological Society, 88, 341 – 356, https://doi.org/10.1175/BAMS-88-3-341, 2007.

Fritts, D. C. and Alexander, M. J.: Gravity wave dynamics and effects in the middle atmosphere, Reviews of Geophysics, 41, https://doi.org/https://doi.org/10.1029/2001RG000106, 2003.

Grubišić, V., Doyle, J. D., Kuettner, J., Mobbs, S., Smith, R. B., Whiteman, C. D., Dirks, R., Czyzyk, S., Cohn, S. A., Vosper, S., Weissmann, M., Haimov, S., De Wekker, S. F. J., Pan, L. L., and Chow, F. K.: The Terrain-Induced Rotor Experiment: A Field Campaign Overview Including Observational Highlights, Bulletin of the American Meteorological Society, 89, 1513–1534, https://doi.org/10.1175/2008BAMS2487.1, 2008.

https://doi.org/10.5194/egusphere-2026-2568
Preprint. Discussion started: 12 August 2026

Hill, M., Calhoun, R., Fernando, H. J. S., Wieser, A., Dörnbrack, A., Weissmann, M., Mayr, G., and Newsom, R.: Coplanar Doppler Lidar Retrieval of Rotors from T-REX, Journal of the Atmospheric Sciences, 67, 713 – 729, https://doi.org/10.1175/2009JAS3016.1, 2010.

Jiang, H. and Edson, J. B.: Characterizing marine atmospheric boundary layer to support offshore wind energy research, in: Journal of Physics: Conference Series, vol. 1452, p. 012027, IOP Publishing, 2020.

Kirinchich, A. et al.: Improving the Understanding and Forecasting of Winds over the Northeast U.S. Shelf: The Third Wind Forecast Improvement Project (WFIP3), Bulletin of the American Meteorological Society, under review, 2026.

Kollias, P., Luke, E., Oue, M., and Lamer, K.: Agile Adaptive Radar Sampling of Fast-Evolving Atmospheric Phenomena Guided by Satellite Imagery and Surface Cameras, Geophysical Research Letters, 47, e2020GL088 440, https://doi.org/https://doi.org/10.1029/2020GL088440, e2020GL088440 2020GL088440, 2020.

Kotamarthi, R., Wang, J., Stock, J., Fytanidis, D. K., Munson, T., Niyogi, D., Muradyan, P., Jackson, R., O'Brien, J., Grover, M., Collis, S., Gonzalez-Meler, M. A., Lee, J., Sharma, A., Wang, S., Kaludi, B., Kaplan, M., Nesbitt, S. W., Martilli, A., Jacob, R., and Negri, C.: Artificial Intelligence–Enabled Digital Twin for U.S. Cities, Bulletin of the American Meteorological Society, 106, E2411 – E2418, https://doi.org/10.1175/BAMS-D-25-0229.1, 2025.

Krishnamurthy, R., Newsom, R. K., Berg, L. K., Xiao, H., Ma, P.-L., and Turner, D. D.: On the estimation of boundary layer heights: a machine learning approach, Atmospheric Measurement Techniques, 14, 4403–4424, https://doi.org/10.5194/amt-14-4403-2021, 2021.

Krishnamurthy, R., Newsom, R. K., Kaul, C. M., Letizia, S., Pekour, M., Hamilton, N., Chand, D., Flynn, D., Bodini, N., and Moriarty, P.: Observations of wind farm wake recovery at an operating wind farm, Wind Energy Science, 10, 361–380, https://doi.org/10.5194/wes-10-361-2025, 2025.

Lamer, K., Luke, E. P., Walsh, B., Andrade, S., Mages, Z., Zhu, Z., Leghart, E., Treserras, B. P., Emrick, A., Kollias, P., Vogelmann, A., and Schoonen, M.: Going Mobile to Address Emerging Climate Equity Needs in the Heterogeneous Urban Environment, Bulletin of the American Meteorological Society, 103, E2069 – E2080, https://doi.org/10.1175/BAMS-D-21-0336.1, 2022.

Lamer, K., Kollias, P., Luke, E. P., Treserras, B. P., Oue, M., and Dolan, B.: Multisensor Agile Adaptive Sampling (MAAS): A Methodology to Collect Radar Observations of Convective Cell Life Cycle, Journal of Atmospheric and Oceanic Technology, 40, 1509 – 1522, https://doi.org/10.1175/JTECH-D-23-0043.1, 2023.

Muradyan, P., Collis, S., O'Brien, J. R., Tuftedal, M., Jackson, R., Raut, B. A., Grover, M., Kaludi, B., Vincent, A. E. S., Wagner, T. J., Sankaran, R., Cho, A., Weart, B., Pal, S., Sullivan, R. C., Anderson, G., Berkelhammer, M., Conrad, N., DuMerer, D., Fytanidis, D. K., Gala, T., Gonzalez-Meler, M. A., Hence, D., Lee, J., Lozano, F., Michnick, J., Miller, W. M., Nesbitt, S., Packman, A. I., Park, S. Y., Saari, C., Shahkarami, S., Wang, J., Wawrzyniak, E., Yocca, D., Zvolanek, E., Beaudry, S., Kotamarthi, R., and Negri, C.: CROCUS Micronet: A Distributed, AI-Enabled Urban Observation System in Chicago, Bulletin of the American Meteorological Society, manuscript under review, 2026.

Newsom, R. K. and Krishnamurthy, R.: Doppler Lidar (DL) Instrument Handbook, Tech. Rep. DOE/SC-ARM-TR-101, DOE Office of Science Atmospheric Radiation Measurement (ARM) User Facility, 2022.

Newsom, R. K., Brewer, W. A., Wilczak, J. M., Wolfe, D. E., Oncley, S. P., and Lundquist, J. K.: Validating precision estimates in horizontal wind measurements from a Doppler lidar, Atmospheric Measurement Techniques, 10, 1229–1240, https://doi.org/10.5194/amt-10-1229-2017, 2017.

O'Connor, E. J., Illingworth, A. J., Brooks, I. M., Westbrook, C. D., Hogan, R. J., Davies, F., and Brooks, B. J.: A Method for Estimating the Turbulent Kinetic Energy Dissipation Rate from a Vertically Pointing Doppler Lidar, and Independent Evaluation from Balloon-Borne

In Situ Measurements, Journal of Atmospheric and Oceanic Technology, 27, 1652 – 1664, https://doi.org/10.1175/2010JTECHA1455.1, 2010.

Park, S., Jackson, R., Kim, Y., Arcomano, T., Raut, B. A., Ferrier, N., and Collis, S.: Automated Lake Breeze Front Identification Using Local Radar Data and Machine Learning Methods, Journal of AI for Earth Systems, submitted, 2026.

Pearson, G., Davies, F., and Collier, C.: An Analysis of the Performance of the UFAM Pulsed Doppler Lidar for Observing the Boundary Layer, Journal of Atmospheric and Oceanic Technology, 26, 240–250, https://doi.org/10.1175/2008JTECHA1128.1, 2009.

Puccioni, M., Wharton, S., De Wekker, S. F. J., Arthur, R. S., Li, T., Liu, Y., Feng, S., Pressel, K., Rai, R. K., Berg, L. K., and Fast, J. D.: Spatio-temporal heterogeneity of the wind resources over a deciduous forest in the U.S. Southeast, Wind Energy Science Discussions [preprint], https://doi.org/10.5194/wes-2025-215, in review, 2025.

Rotach, M. W., Serafin, S., Ward, H. C., Arpagaus, M., Colfescu, I., Cuxart, J., Wekker, S. F. J. D., Grubišic, V., Kalthoff, N., Karl, T., Kirshbaum, D. J., Lehner, M., Mobbs, S., Paci, A., Palazzi, E., Bailey, A., Schmidli, J., Wittmann, C., Wohlfahrt, G., and Zardi, D.: A Collaborative Effort to Better Understand, Measure, and Model Atmospheric Exchange Processes over Mountains, Bulletin of the American Meteorological Society, 103, E1282 – E1295, https://doi.org/10.1175/BAMS-D-21-0232.1, 2022.

Shaw, W., Berg, L., Debnath, M., Deskos, G., Draxl, C., Ghate, V., Hasager, C., Kotamarthi, R., Mirocha, J., Muradyan, P., et al.: Scientific challenges to characterizing the wind resource in the marine atmospheric boundary layer, Wind Energy Science Discussions, 2022, 1–47, 2022.

Smalikho, I., Köpp, F., and Rahm, S.: Measurement of Atmospheric Turbulence by 2-μm Doppler Lidar, Journal of Atmospheric and Oceanic Technology, 22, 1733 – 1747, https://doi.org/10.1175/JTECH1815.1, 2005.

Smalikho, I. N. and Banakh, V. A.: Accuracy of estimation of the turbulent energy dissipation rate from wind measurements with a conically scanning pulsed coherent Doppler lidar. Part I. Algorithm of data processing, Atmospheric and Oceanic Optics, 26, 404–410, https://doi.org/10.1134/S102485601305014X, 2013.

Smalikho, I. N. and Banakh, V. A.: Measurements of wind turbulence parameters by a conically scanning coherent Doppler lidar in the atmospheric boundary layer, Atmospheric Measurement Techniques, 10, 4191–4208, https://doi.org/10.5194/amt-10-4191-2017, 2017.

Stull, R. B.: An introduction to boundary layer meteorology, vol. 13, Springer Science & Business Media, 2012.

Wang, L., Mačak, M. B., Stanič, S., Patruno, L., Dong, W., and Chen, D.: Orography-Induced Atmospheric Small-Scale Waves During Bora Using Lidar Observations and Numerical Simulations, Geophysical Research Letters, 52, e2024GL112 400, https://doi.org/https://doi.org/10.1029/2024GL112400, e2024GL112400 2024GL112400, 2025.

Wang, Q., Alappattu, D. P., Billingsley, S., Blomquist, B., Burkholder, R. J., Christman, A. J., Creegan, E. D., de Paolo, T., Eleuterio, D. P., Fernando, H. J. S., Franklin, K. B., Grachev, A. A., Haack, T., Hanley, T. R., Hocut, C. M., Holt, T. R., Horgan, K., Jonsson, H. H., Hale, R. A., Kalogiros, J. A., Khelif, D., Leo, L. S., Lind, R. J., Lozovatsky, I., Planella-Morato, J., Mukherjee, S., Nuss, W. A., Pozderac, J., Rogers, L. T., Savelyev, I., Savidge, D. K., Shearman, R. K., Shen, L., Terrill, E., Ulate, A. M., Wang, Q., Wendt, R. T., Wiss, R., Woods, R. K., Xu, L., Yamaguchi, R. T., and Yardim, C.: CASPER: Coupled Air–Sea Processes and Electromagnetic Ducting Research, Bulletin of the American Meteorological Society, 99, 1449 – 1471, https://doi.org/10.1175/BAMS-D-16-0046.1, 2018.

Wekker, S. F. J. D. and Mayor, S. D.: Observations of Atmospheric Structure and Dynamics in the Owens Valley of California with a Ground-Based, Eye-Safe, Scanning Aerosol Lidar, Journal of Applied Meteorology and Climatology, 48, 1483 – 1499, https://doi.org/10.1175/2009JAMC2034.1, 2009.

https://doi.org/10.5194/egusphere-2026-2568
Preprint. Discussion started: 12 August 2026

Wharton, S., Ma, S., Baldocchi, D., Falk, M., Newman, J., Osuna, J., and Bible, K.: Influence of regional nighttime atmospheric regimes on canopy turbulence and gradients at a closed and open forest in mountain-valley terrain, Agricultural and Forest Meteorology, 237, 18–29, 2017.

Whiteman, C. D.: Observations of Thermally Developed Wind Systems in Mountainous Terrain, pp. 5–42, American Meteorological Society, Boston, MA, https://doi.org/10.1007/978-1-935704-25-6_2, 1990.

Wilczak, J., Finley, C., Freedman, J., Cline, J., Bianco, L., Olson, J., Djalalova, I., Sheridan, L., Ahlstrom, M., Manobianco, J., Zack, J., Carley, J. R., Benjamin, S., Coulter, R., Berg, L. K., Mirocha, J., Clawson, K., Natenberg, E., and Marquis, M.: The Wind Forecast Improvement Project (WFIP): A Public–Private Partnership Addressing Wind Energy Forecast Needs, Bulletin of the American Meteorological Society, 96, 1699 – 1718, https://doi.org/10.1175/BAMS-D-14-00107.1, 2015.

Wilczak, J. M., Stoelinga, M., Berg, L. K., Sharp, J., Draxl, C., McCaffrey, K., Banta, R. M., Bianco, L., Djalalova, I., Lundquist, J. K., Muradyan, P., Choukulkar, A., Leo, L., Bonin, T., Pichugina, Y., Eckman, R., Long, C. N., Lantz, K., Worsnop, R. P., Bickford, J., Bodini, N., Chand, D., Clifton, A., Cline, J., Cook, D. R., Fernando, H. J. S., Friedrich, K., Krishnamurthy, R., Marquis, M., McCaa, J., Olson, J. B., Otarola-Bustos, S., Scott, G., Shaw, W. J., Wharton, S., and White, A. B.: The Second Wind Forecast Improvement Project (WFIP2): Observational Field Campaign, Bulletin of the American Meteorological Society, 100, 1701 – 1723, https://doi.org/10.1175/BAMS-D-18-0035.1, 2019.